Next-to-next-to-leading order matching of beauty-charmed meson B_c and B_c^* decay constants

Wei Tao,[‡] Ruilin Zhu,[*] and Zhen-Jun Xiao[†]

Department of Physics and Institute of Theoretical Physics, Nanjing Normal University, Nanjing, Jiangsu 210023, China

(Received 3 October 2022; accepted 14 December 2022; published 30 December 2022)

We present the next-to-next-to-leading order (NNLO) quantum chromodynamics (QCD) corrections to the decay constants for both the pseudoscalar B_c meson and the vector B_c^* meson in the nonrelativistic QCD (NRQCD) effective theory. The explicit NNLO calculations prove that the B_c decay constant from the pseudoscalar current is identical with the B_c decay constant from the axial-vector current. The NNLO result for the vector decay constant of B_c^* meson is novel. Combining this result with the latest extraction of the NRQCD long-distance matrix elements of B_c and B_c^* meson, we calculate and show the theoretical predictions for the branching ratios of the leptonic decays $B_c^+/B_c^{*+} \to l^+\nu_l$ with $l^+ = (e^+, \mu^+, \tau^+)$. In addition, the novel anomalous dimension for the flavor-changing heavy quark vector current in the NRQCD effective theory is helpful to investigate the threshold behaviors of the two different heavy quarks.

DOI: 10.1103/PhysRevD.106.114037

I. INTRODUCTION

The beauty-charmed meson $B_c(1S)$ was first discovered in proton antiproton colliders by the CDF Collaboration [1]. The second new member in beauty-charmed meson family, i.e., $B_c(2S)$, was discovered in the LHC experiment by ATLAS Collaboration [2]. Five years later, the $B_c(2S)$ state was confirmed by both CMS and LHCb Collaborations, the new vector member $B_c^*(2S)$ was first reported by these two collaborations [3,4]. Up to now, no other member in the beauty-charmed meson family have been observed in particle physics experiments although more beauty-charmed mesons have been predicted in many theoretical models.

Unlike the heavy quarkonium, the experimental measurements of the B_c meson family are not easy since they are composed of two different heavy-flavor quarks, and the ground state $B_c(1S)$ only decays weakly into other lighter particles. Although there are 48 possible decay channels (as listed in the latest review of particle physics) which have been reported in experiments, no one has an experimental measurement of the absolute branching ratios [5].[1]

To promote the determination of the absolute branching ratios of the B_c mesons, a careful investigate the fundamental properties of the decay behaviors is required. In other words, we need first to have a good knowledge of the decay constants for the B_c meson family. In principle, the decay constants for the B_c mesons are nonperturbative yet universal physical quantities. Lattice QCD should be a good method to determine the relevant decay constants from the first principles of QCD, however the lattice QCD studies on the B_c mesons are lesser because the B_c mesons include two different kinds of the heavy quarks and the doubly heavy quark systems are not easy to be simulated in current lattice studies.[2]

The nonrelativistic QCD (NRQCD) effective theory provides a systematical and accurate framework to study the doubly heavy quark systems [9]. In this effective theory, the heavy quark mass provides a natural factorization scale. The short-distance physics above the heavy quark mass can be perturbatively calculated and factorized into the Wilson coefficients while the long-distance physics below the heavy quark mass goes into the long-distance matrix

[*]Corresponding author.
rlzhu@njnu.edu.cn

[†]Corresponding author.
xiaozhenjun@njnu.edu.cn

[‡]taowei@njnu.edu.cn

[1]An exception is the absolute branching ratio of $B_c^+ \to \chi_{c0}\pi^+$, which is extracted by particle data group after inputting the bottom quark fragmentation probability into B meson and the LHCb data.

[2]There is a 2σ tension for the B_c decay constant between the ETM lattice result and the HPQCD lattice result [6,7]. Based on the heavy highly improved staggered quark approach, HPQCD has also performed lattice QCD simulations on the vector and axial-vector form factors of $B_c \to J/\psi$ [8].

elements (LDMEs). Within the NRQCD effective theory, the decay constants for the B_c mesons can be further factorized as the short-distance matching coefficients and the corresponding NRQCD LDMEs.

Using the NRQCD effective theory, the next-to-leading order (NLO) corrections including both the strong coupling constant correction at the order α_s and the relative velocity correction at the order v^2 to the axial-vector decay constant of the B_c meson which were first calculated by Braaten and Fleming [10], after a systematical study of the B_c meson at the leading order (LO) by Chang and Chen [11]. Using the resummation technique, the NLO correction including all order relative velocity corrections to the axial-vector decay constant of the B_c meson and the vector decay constant of B_c^* was estimated by Lee *et al.* [12]. The next-to-next-to-leading order (NNLO) correction at order α_s^2 to the axial-vector decay constant of B_c meson was first investigated by Onishchenko and Veretin [13]. However, the full analytical expression of the axial-vector decay constant of B_c meson at the NNLO accuracy was accomplished by Chen and Qiao [14]. Very recently, the numerical calculation of the axial-vector decay constant of B_c meson at the NNNLO accuracy was done by Feng *et al.* [15]. Other higher-order calculations on doubly heavy quark system and phenomenological studies on B_c system can be found, for example, in the literature [16–36].

In this paper, we will calculate the pseudoscalar (P) decay constant $f^p_{B_c}$ of B_c meson and the vector (V) decay constant $f^v_{B_c^*}$ of B_c^* meson at the NNLO accuracy within the NRQCD effective theory. By an explicit calculation, we can investigate the relation among various decay constants defined by the different flavor-changing heavy quark currents. It is easy to prove that $f^p_{B_c}$ is identical to the axial-vector (A) decay constant $f^a_{B_c}$ of B_c meson. The NNLO results of the vector decay constant $f^v_{B_c^*}$ are novel. Combining with the latest extraction of the NRQCD LDMEs, we present our theoretical predictions for the branching ratios of the leptonic decays $B_c^+/B_c^{*+} \to l^+\nu_l$ with $l^+ = (e^+, \mu^+, \tau^+)$. The analytical and numerical results of the short-distance matching coefficients $\mathcal{C}_{p,v}$ are also useful to analyze the threshold behaviors when two different heavy quarks are close to each other.

In addition, we obtain a novel anomalous dimension for the flavor-changing heavy quark vector current at the NNLO accuracy in the NRQCD effective theory. This anomalous dimension is related to the renormalization behaviors of the vector current with two different heavy quarks in NRQCD.

The paper is arranged as follows. In Sec. II, we give the definitions of the decay constants of the P, A, and V currents for the mesons B_c and B_c^* in both the full QCD theory and the NRQCD effective theory. We then present the matching formulas for the decay constants in the NRQCD effective theory. In Sec. III, we present the calculation methods and the calculation procedures for the short-distance matching coefficients $\mathcal{C}_{p,v}$. In Sec. IV, we give the final NNLO results of $\mathcal{C}_{p,v}$ and the decay constants of the B_c and B_c^* mesons. We also perform a phenomenological analysis of the leptonic decays of B_c and B_c^* mesons. We conclude at the end of the paper.

II. MATCHING FORMULAS

Though the B_c meson leptonic decay is dominated by the virtual W boson with a $V-A$ weak interaction in the Standard Model (SM), one can freely define the B_c meson decay constants by different flavor-changing currents. Thus one can define the pseudoscalar and vector B_c meson decay constants by the full QCD matrix elements

$$\langle 0|\bar{b}\gamma^\mu\gamma_5 c|B_c(P)\rangle = i f^a_{B_c} P^\mu, \tag{1}$$

$$\langle 0|\bar{b}\gamma_5 c|B_c(P)\rangle = i f^p_{B_c} m_{B_c}, \tag{2}$$

$$\langle 0|\bar{b}\gamma^\mu c|B_c^*(P,\varepsilon)\rangle = f^v_{B_c^*} m_{B_c^*}\varepsilon^\mu, \tag{3}$$

where $|B_c(P)\rangle$ and $|B_c^*(P,\varepsilon)\rangle$ are respectively the states of the pseudoscalar and vector B_c mesons with the four-momentum P, while ε^μ is the polarization vector of the B_c^* meson. In full QCD, the standard covariant normalization of the hadron state is $\langle B_c(P')|B_c(P)\rangle = (2\pi)^3 2P^0\delta^3(P'-P)$. The imaginary unit in the right hand of Eqs. (1) and (2) is added to make sure the decay constant f_{B_c} is real and positive. Note that other decay constants for B_c family with scalar and tensor currents are not considered in this paper. Using the heavy quark equation of motion, one can easily get the identity $f^a_{B_c} = f^p_{B_c}$. Thus, we only need to calculate two decay constants, $f^p_{B_c}$ and $f^v_{B_c^*}$, here.

The above decay constants of B_c mesons are nonperturbative observables in full QCD and rely on a nonperturbative calculation; however, the two heavy quark system B_c is not well-simulated at current lattice QCD and these physical quantities are rarely investigated in first principals theory of QCD.

In the NRQCD effective theory, the decay constants of B_c mesons can be further factorized into perturbatively calculable short-distance coefficients with the corresponding nonperturbative LDMEs. Thus, one can write the following matching formula at leading order in the relative velocity expansion

$$f^p_{B_c} = \sqrt{\frac{2}{m_{B_c}}}\mathcal{C}_p(m_b, m_c, \mu_f)\langle 0|\chi_b^\dagger\psi_c|B_c(\mathbf{P})\rangle(\mu_f) + \mathcal{O}(v^2), \tag{4}$$

$$f^v_{B_c^*} = \sqrt{\frac{2}{m_{B_c^*}}}\mathcal{C}_v(m_b, m_c, \mu_f)\langle 0|\chi_b^\dagger\boldsymbol{\sigma}\cdot\varepsilon\psi_c|B_c^*(\mathbf{P})\rangle(\mu_f) + \mathcal{O}(v^2), \tag{5}$$

where μ_f is the NRQCD factorization scale which appears in the short-distance coefficients at two-loop calculation and will be canceled between the short-distance coefficients and the NRQCD LDMEs. In QCD perturbative calculations, the decay constants will depend on the renormalization scale μ in fixed-order accuracy and will become renormalization-scale independent after summing up all-order contributions.

III. CALCULATION OF THE MATCHING COEFFICIENTS

In this section, we present our calculation procedures for the decay constants of pseudoscalar and vector B_c mesons within the NRQCD approach. According to the above matching formulas, the matching coefficients $\mathcal{C}_p$ and $\mathcal{C}_v$ can be obtained by the calculations of both the full QCD matrix elements and the NRQCD matrix elements. At the leading order, the matching coefficients $\mathcal{C}_p$ and $\mathcal{C}_v$ are set as $\mathcal{C}_p = \mathcal{C}_v = 1$, which can also be done after the nonrelativistic expansion of heavy quark current. The Feynman diagrams for B_c and B_c^* decay constants up to two-loop order are plotted in Fig. 1.

Our higher-order calculation of the matching coefficients consists of the following steps. First, we use FeynCalc [37] to obtain the Feynman diagrams and the corresponding Feynman amplitudes. By $Apart [38], we decompose every Feyman amplitude into several Feynman integral families. Second, we use KIRA [39]/FIRE [40]/FiniteFlow [41] based on integration by parts (IBP) [42] to reduce every Feynman integral family to master integral family. Third, based on symmetry among different integral families and using KIRA +FIRE+*Mathematica* code, we can realize integral reduction among different integral families, and further on, the reduction from all of master integral families to the minimal master integral families. Last, we use AMFlow [43], which is a proof-of-concept implementation of the auxiliary mass flow method [44], equipped with KIRA/FiniteFlow to calculate the minimal master integral families one by one.

In order to obtain the high-order coefficient $\mathcal{C}_J$ with $J = (p, v)$, one has to perform the conventional renormalization procedure, which is similar to what is shown in

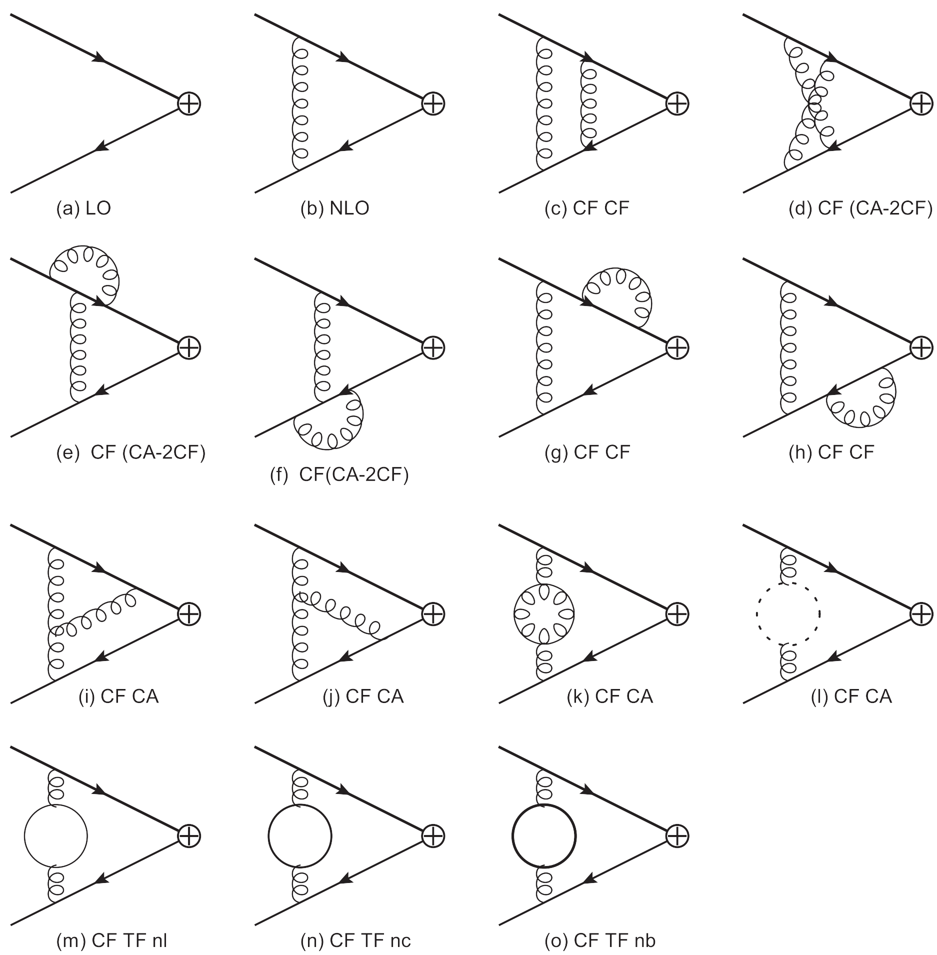

FIG. 1. The Feynman diagrams labeled with corresponding color factor for B_c and B_c^* decay constants up to two-loop order. The cross "$\oplus$" implies the insertion of certain heavy flavor-changing current. The thinnest, thick, thickest solid circles represent n_l massless quark loop, n_c quark loop with mass m_c, n_b quark-loop with mass m_b, respectively. In this paper, we set $n_b = n_c = 1$.

Refs. [14,45–47], i.e., $Z_J Z_{2,b}^{\frac{1}{2}} Z_{2,c}^{\frac{1}{2}} \Gamma_J = \mathcal{C}_J \tilde{Z}_J^{-1} \tilde{Z}_{2,b}^{\frac{1}{2}} \tilde{Z}_{2,c}^{\frac{1}{2}} \tilde{\Gamma}_J$, where the left part in the equation represents the renormalization of the full QCD current while the right part represents the renormalization of the NRQCD current. Z_J and $\tilde{Z}_J^{-1}$ are the renormalization constants for the full QCD and NRQCD flavor-changing currents, respectively. Here, $Z_a = Z_v = 1$, $Z_p = (m_b Z_{m,b} + m_c Z_{m,c})/(m_b + m_c)$, and $\tilde{Z}_{2,b} = \tilde{Z}_{2,c} = 1$. Equivalently, we can also use the diagrammatic renormalization method [48], which contains two-loop diagrams and three kinds of counterterm diagrams, i.e., the tree diagram inserted with one α_s^2-order counterterm vertex, the tree diagram inserted with two α_s-order counterterm vertexes (vanishing), and a one-loop diagram inserted with one α_s-order counterterm vertex.

We want to mention that all contributions have been evaluated for the general gauge parameter ξ, and the final results for the matching coefficients are all independent of ξ, which constitutes an important check on our calculation. In the calculation of two-loop diagrams, we allow for one b quark, one c quark, and n_l massless quarks in the quark loop. Up to two-loop order, the most complicated renormalization constants are the on shell mass and wave function renormalization constants allowing for two different nonzero quark masses [49,50], and the analytical expressions of these constants $(Z_{2,b}, Z_{2,c})$ and $(Z_{m,b}, Z_{m,c})$ are presented in the Appendix.

After renormalization, the results of the short-distance matching coefficients $\mathcal{C}_J$ can be written as [15]

$$\begin{aligned}
&\mathcal{C}_J(\mu_f, \mu, m_b, x) \\
&= 1 + \frac{\alpha_s^{(n_f)}(\mu)}{\pi} \mathcal{C}_J^{(1)}(x) \\
&+ \left(\frac{\alpha_s^{(n_f)}(\mu)}{\pi}\right)^2 \left(\mathcal{C}_J^{(1)}(x) \frac{\beta_0^{(n_f)}}{4} \ln\frac{\mu^2}{m_b^2} + \frac{\gamma_J^{(2)}(x)}{2} \ln\frac{\mu_f^2}{m_b^2}\right. \\
&+ C_F^2 \mathcal{C}_J^{FF}(x) + C_F C_A \mathcal{C}_J^{FA}(x) + C_F T_F n_l \mathcal{C}_J^{FL}(x) \\
&\left. + C_F T_F \mathcal{C}_J^{FH}(x)\right) + \mathcal{O}(\alpha_s^3),
\end{aligned} \tag{6}$$

where $C_F = 4/3, C_A = 3$ and $T_F = 1/2$ are QCD constants, and the dimensionless parameter x representing the ratio of two heavy quark masses is

$$x = \frac{m_c}{m_b}, \tag{7}$$

and the first two coefficients in β functions for α_s are

$$\beta_0^{(n_f)} = (11/3)C_A - (4/3)T_F n_f, \tag{8}$$

$$\beta_1^{(n_f)} = (34/3)C_A^2 - (20/3)C_A T_F n_f - 4 C_F T_F n_f. \tag{9}$$

We have considered the contributions from heavy charm and bottom quark loops in the gluon self-energy Feynman diagrams, which however are decoupled in the NRQCD effective theory. Thus we apply the following decoupling relation as given in Refs. [51–55] to translate $\alpha_s^{(n_f)}(\mu)$ involving massive flavors to $\alpha_s^{(n_l)}(\mu)$ involving n_l massless flavors only,

$$\begin{aligned}
\alpha_s^{(n_f)}(\mu) = \alpha_s^{(n_l)}(\mu)\Bigg(1 + \frac{\alpha_s^{(n_l)}(\mu)}{\pi} T_F \bigg(\frac{n_b}{3}\ln\frac{\mu^2}{m_b^2} \\
+ \frac{n_c}{3}\ln\frac{\mu^2}{m_c^2} + \mathcal{O}(\epsilon)\bigg) + \mathcal{O}(\alpha_s^2)\Bigg),
\end{aligned} \tag{10}$$

where $n_f = n_l + n_b + n_c$. In our numerical calculation, $n_b = n_c = 1$, $n_l = 3$ are fixed through the decoupling region from $\mu = 1$ GeV to $\mu = 6.25$ GeV and the following results for strong coupling constant running [56–60] are used, i.e.,

$$\begin{aligned}
\alpha_s^{(n_l)}(\mu_f) &= \left(\frac{\mu}{\mu_f}\right)^{2\epsilon} \alpha_s^{(n_l)}(\mu) + \mathcal{O}(\alpha_s^2), \\
\alpha_s^{(n_l)}(\mu) &= \frac{4\pi}{\beta_0^{(n_l)} \ln\frac{\mu^2}{\Lambda_{\rm QCD}^{(n_l)\,2}}} \left(1 - \frac{\beta_1^{(n_l)} \ln\ln\frac{\mu^2}{\Lambda_{\rm QCD}^{(n_l)\,2}}}{\beta_0^{(n_l)2} \ln\frac{\mu^2}{\Lambda_{\rm QCD}^{(n_l)\,2}}}\right) \\
&\quad + \mathcal{O}\left(\frac{1}{\ln^3\frac{\mu^2}{\Lambda_{\rm QCD}^{(n_l)\,2}}}\right),
\end{aligned} \tag{11}$$

where the typical QCD scale $\Lambda_{\rm QCD}^{(n_l=3)} = 336$ MeV can be iteratively determined from an initial input of $\alpha_s^{(n_f=5)}(m_Z) = 0.1179$.

The explicit analytical calculations of the NLO Feynman diagrams give the NLO short-distance matching coefficients

$$\mathcal{C}_p^{(1)}(x) = \frac{3}{4} C_F \left(\frac{x-1}{x+1}\ln x - 2\right), \tag{12}$$

$$\mathcal{C}_v^{(1)}(x) = \frac{3}{4} C_F \left(\frac{x-1}{x+1}\ln x - \frac{8}{3}\right). \tag{13}$$

Note that the analytical expressions of $\mathcal{C}_p^{(1)}(x)$ and $\mathcal{C}_v^{(1)}(x)$ are consistent with those given in Refs. [10,12].

At NNLO, the direct results of the short-distance matching coefficients are still IR divergent after performing the UV renormalization for the QCD current. This is due to the UV divergence in the NRQCD LDMEs at NNLO. The NRQCD factorization theory makes sure the two kinds of divergences are canceled order by order.

By matching, we obtain the renormalization constants for different NRQCD currents as follows [15]:

$$\tilde{Z}_J = 1 - \left(\frac{\alpha_s^{(n_l)}(\mu_f)}{\pi}\right)^2 \frac{\gamma_J^{(2)}(x)}{4\epsilon} + \mathcal{O}(\alpha_s^3), \qquad (14)$$

where μ_f is the NRQCD factorization scale, and the coefficients $\gamma_J^{(2)}(x)$ with $J = (p, v)$ are of the following form

$$\gamma_p^{(2)}(x) = -\pi^2\left(\frac{C_F C_A}{2} + \frac{(1+6x+x^2)C_F^2}{2(1+x)^2}\right), \qquad (15)$$

$$\gamma_v^{(2)}(x) = -\pi^2\left(\frac{C_F C_A}{2} + \frac{(3+2x+3x^2)C_F^2}{6(1+x)^2}\right). \qquad (16)$$

The corresponding anomalous dimension γ_J is related to $\tilde{Z}_J$ by [13,61]

$$\gamma_J = \frac{d\ln\tilde{Z}_J}{d\ln\mu_f} = \left(\frac{\alpha_s^{(n_l)}(\mu_f)}{\pi}\right)^2 \gamma_J^{(2)}(x) + \mathcal{O}(\alpha_s^3), \qquad (17)$$

where $\alpha_s^{(n_l)}(\mu_f)$ can be related to $\alpha_s^{(n_l)}(\mu)$ by the running equation in order to performing the matching between QCD and NRQCD currents [60], as described in Eq. (11).

Note that the anomalous dimension $\gamma_v^{(2)}(x)$ is a novel result for the two different heavy quarks meson. In the case of $x = 1$, the result is consistent with the previous calculation, for example in Ref. [45]. By the renormalization of the UV divergence in the NRQCD LDMEs at NNLO, the extra IR-divergences in short-distance coefficients can be exactly canceled. Thus, we finally get the finite results for the matching coefficients.

IV. NUMERICAL RESULTS AND DISCUSSIONS

In this section, we will give the numerical results for the matching coefficients $\mathcal{C}_J(\mu_f, \mu, m_b, x)$ with $J = p$, v at the NNLO accuracy. The subcoefficients $\mathcal{C}_J^{FF}$, $\mathcal{C}_J^{FA}$, $\mathcal{C}_J^{FL}$, and $\mathcal{C}_J^{FH}$ classified by different color/flavor structures in Eq. (6) are functions which only depend on the heavy quark mass ratio $x = m_c/m_b$. At the physical heavy quark mass ratio $x_0 = 1.5/4.75$ [62–64], we obtained the following highly accurate numerical results with about 30-digit precision for the all four kinds of subcoefficients.

$$\mathcal{C}_p^{FF}(x_0) = -18.1856109097151570253549607713, \qquad (18)$$

$$\mathcal{C}_p^{FA}(x_0) = -11.9709902751165587736864132992, \qquad (19)$$

$$\mathcal{C}_p^{FL}(x_0) = 0.461971258745060837844427133019, \qquad (20)$$

$$\mathcal{C}_p^{FH}(x_0) = 1.64553283592627680478382129760. \qquad (21)$$

$$\mathcal{C}_v^{FF}(x_0) = -15.8653228579431784031838005865, \qquad (22)$$

$$\mathcal{C}_v^{FA}(x_0) = -11.0678680506800630685188604612, \qquad (23)$$

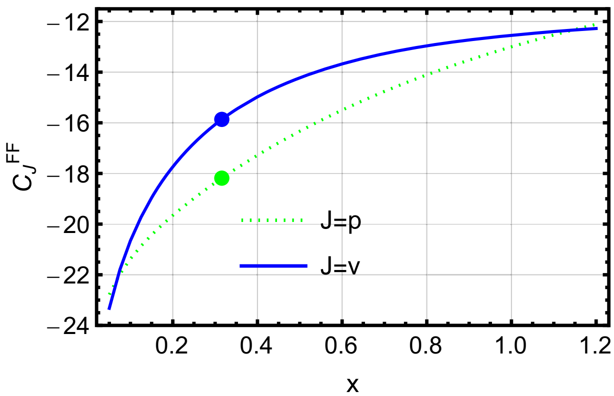

FIG. 2. The profile of subcoefficient $\mathcal{C}_J^{FF}(x)$ dependence on heavy quark mass ratio $x = \frac{m_c}{m_b}$ with $x \in [0.05, 1.2]$. $J = p$ represents the subcoefficient for the pseudoscalar current while $J = v$ represents the subcoefficient for the vector current. According to color/flavor structure, this subcoefficient has a prefactor C_F^2 for both the pseudoscalar current and the vector current. The green and blue dots correspond to the results at physical heavy quark mass ratio with $x_0 = \frac{1.5}{4.75}$.

$$\mathcal{C}_v^{FL}(x_0) = 1.08196339731790945235792891668, \qquad (24)$$

$$\mathcal{C}_v^{FH}(x_0) = 1.87201601140852309779426933441. \qquad (25)$$

In order to investigate the heavy quark mass dependence of the matching coefficients, we vary the heavy quark mass ratio x from $x_{\min} = 0.05$ to $x_{\max} = 1.2$. And we plotted the heavy quark mass ratio x dependence for the subcoefficients $\mathcal{C}_J^{FF}$, $\mathcal{C}_J^{FA}$, $\mathcal{C}_J^{FL}$, and $\mathcal{C}_J^{FH}$ in Figs. 2–5, respectively.

In these diagrams, $J = p$ represents the sub-coefficient for the pseudoscalar current while $J = v$ represents the subcoefficient for the vector current. From the curves in Figs. 2–5, one can see that the subcoefficients are close to each other for both P and V currents, except $\mathcal{C}_J^{FL}$. The subcoefficients $\mathcal{C}_J^{FF}$ and $\mathcal{C}_J^{FA}$ increase gradually with the increase of the heavy quark mass ratio $x = m_c/m_b$, while

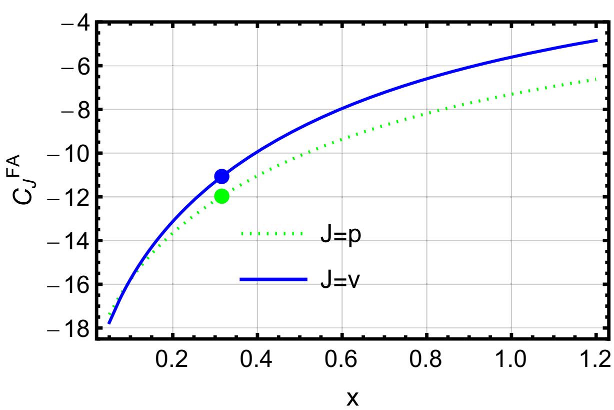

FIG. 3. The same as Fig. 2, but for the profile of subcoefficient $\mathcal{C}_J^{FA}(x)$ which has a prefactor $C_F C_A$.

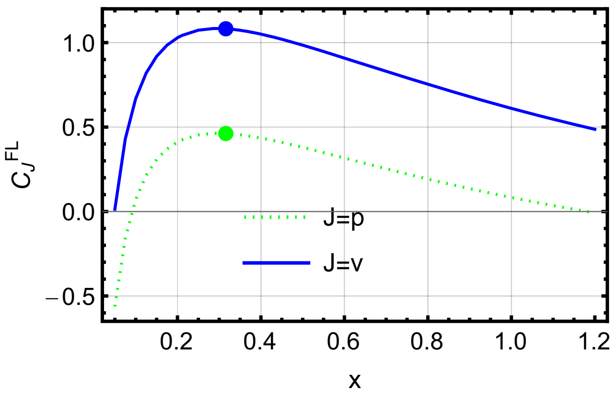

FIG. 4. The same as Fig. 2, but for the profile of subcoefficient $\mathcal{C}_J^{FL}(x)$ which has a prefactor $C_F T_F n_l$.

$\mathcal{C}_J^{FL}$ and $\mathcal{C}_J^{FH}$ first increase and then reduce with the increase of x.

By fixing the renormalization scale $\mu = m_b = 4.75$ GeV, $m_c = 1.5$ GeV, $x_0 = m_c/m_b = 1.5/4.75$, and setting the factorization scale $\mu_f = 1.2$ GeV, the matching coefficients $\mathcal{C}_p$ and $\mathcal{C}_v$ as defined in Eq. (6) will reduce to

$$\mathcal{C}_p(x_0) = 1 - 1.40061\frac{\alpha_s^{(n_l=3)}(m_b)}{\pi} - 30.69707\left(\frac{\alpha_s^{(n_l=3)}(m_b)}{\pi}\right)^2 + \mathcal{O}(\alpha_s^3), \quad (26)$$

$$\mathcal{C}_v(x_0) = 1 - 2.06727\frac{\alpha_s^{(n_l=3)}(m_b)}{\pi} - 33.56657\left(\frac{\alpha_s^{(n_l=3)}(m_b)}{\pi}\right)^2 + \mathcal{O}(\alpha_s^3). \quad (27)$$

By using the definitions in Eq. (6), we calculate the matching coefficients $\mathcal{C}_p(\mu)$ and $\mathcal{C}_v(\mu)$ and present our theoretical predictions in the Figs. 6 and 7. In these two figures, we show the μ-dependence of both $\mathcal{C}_p(\mu)$ and $\mathcal{C}_v(\mu)$ at the LO (the dot-dashed line), NLO (the dashed curve) and NNLO (the solid curve) accuracy by varying μ in the range $1.5 \le \mu \le 6.2$ GeV. The uncertainties of the theoretical predictions at the NLO and NNLO level come from the errors of the input parameters $\mu_f = 1.2^{+0.3}_{-0.2}$ GeV, $m_b = 4.75 \pm 0.5$ GeV and $m_c = 1.5 \pm 0.5$ GeV, while the individual errors are combined in addition.

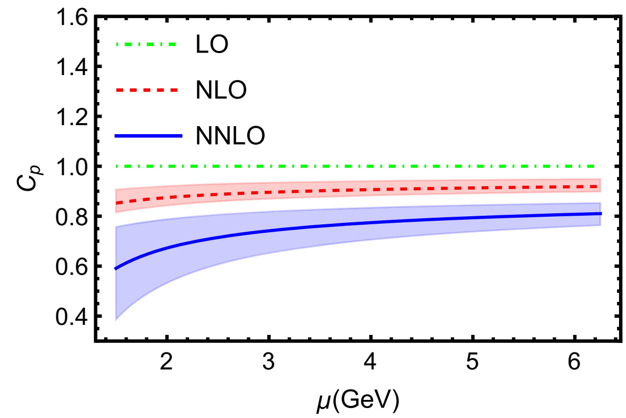

FIG. 6. The μ-dependence of the matching coefficient $\mathcal{C}_p(\mu)$ at the LO, NLO and NNLO accuracy. The error bands show the total theoretical uncertainty. For details see the text.

From Figs. 6 and 7 one can see the following points:

(1) At the LO, we set $\mathcal{C}_p = \mathcal{C}_v = 1$, and both of them are μ-independent.

(2) At the NLO, the QCD corrections bring relatively weak μ-dependence of these two matching coefficients. Because of the absence of explicit μ-dependence in $\mathcal{C}_J^{(1)}(x)$, the μ-dependence of the NLO results is only from $\alpha_s^{(n_f)}(\mu)$. According to the renormalization group equation of the strong coupling constant, the μ-dependence at the NLO is then at the order of $\mathcal{O}(\alpha_s^2)$.

(3) At the NNLO, the μ-dependence includes two aspects. On the one hand, the μ-dependence of

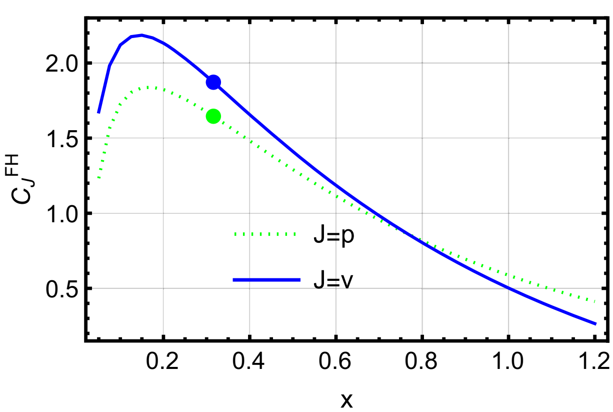

FIG. 5. The same as Fig. 2, but for the profile of subcoefficient $\mathcal{C}_J^{FH}(x)$ which has a prefactor $C_F T_F$.

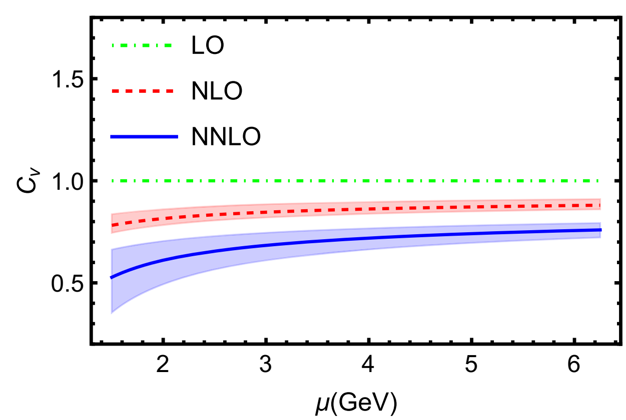

FIG. 7. The same as Fig. 6, but for the matching coefficient $\mathcal{C}_v(\mu)$.

TABLE I. The theoretical predictions for the matching coefficients $\mathcal{C}_{p,v}$ at the NLO and NNLO level. For details of the choice of the input parameters see the text.

NLO
$C_p = 0.9117 \pm 0(\mu_f)^{+0.0072}_{-0.0160}(\mu)^{+0.0061}_{-0.0064}(m_b)^{-0.0156}_{+0.0263}(m_c)$
$C_v = 0.8697 \pm 0(\mu_f)^{+0.0107}_{-0.0236}(\mu)^{+0.0061}_{-0.0064}(m_b)^{-0.0156}_{+0.0263}(m_c)$
NNLO
$C_p = 0.7897^{-0.0310}_{+0.0253}(\mu_f)^{+0.0206}_{-0.0482}(\mu)^{+0.0119}_{-0.0133}(m_b)^{+0.0149}_{-0.0141}(m_c)$
$C_v = 0.7363^{-0.0234}_{+0.0191}(\mu_f)^{+0.0230}_{-0.0526}(\mu)^{+0.0106}_{-0.0526}(m_b)^{+0.0117}_{+0.0121}(m_c)$

the NLO results at the order of $\mathcal{O}(\alpha_s^2)$ can be completely canceled by those from the NNLO corrections, then the left μ-dependence of the NNLO results is at the $\mathcal{O}(\alpha_s^3)$ order. On the other hand, the renormalization scale-independent coefficients such as $C_J^{FA}(x)$ and $\ln(\mu_f^2/m_b^2)$ in front of the strong coupling constant squared α_s^2 in Eq. (6) are not small in these kinds of process, which will lead to a large μ-dependence at the $\mathcal{O}(\alpha_s^3)$ order, especially in the low μ region, as can be seen easily in Figs. 6 and 7.

(4) The μ-dependence of the matching coefficients $C_p(\mu)$ and $C_v(\mu)$ at the NNLO level is therefore not reduced compared with those at the NLO level. We will leave the further investigation of this problem for future work.

In Table I, we list the explicit numerical predictions of the matching coefficients $\mathcal{C}_{p,v}$ at the LO, NLO, and NNLO accuracy, where the uncertainties from the four input parameters also be listed separately. The central values of $\mathcal{C}_{p,v}$ are calculated by using the physical values of $\mu_f = 1.2$ GeV, $\mu = 4.75$ GeV, $m_b = 4.75$ GeV, and $m_c = 1.5$ GeV. The four errors are estimated by varying μ_f from 1.5 GeV to 1 GeV, μ from 6.25 GeV to 3 GeV, m_b from 5.25 GeV to 4.25 GeV, and m_c from 2 GeV to 1 GeV, respectively. From Table I, one can see that the two major uncertainties come from the error of μ_f and μ at the NNLO level.

Note that the matching coefficients are from short-distance effects and only rely on the QCD currents. These matching coefficients do not depend on the meson states. In fact, the matching coefficient $\mathcal{C}_a$ depends on the components ($\mu = 0, i$) of the axial-vector current $\bar{b}\gamma^\mu\gamma_5 c$. At the leading order, in powers of the relative velocity, the nontrival contribution is from the time-component, i.e., $\mathcal{C}_a = \mathcal{C}_{(a,\mu=0)} = \mathcal{C}_{(a,0)}$. The explicit analytical expression for $\mathcal{C}_{(a,0)}$ is given in Ref. [14] at the NNLO accuracy and the numerical results for $\mathcal{C}_{(a,0)}$ are given in Ref. [15] at the NNNLO accuracy. Our results are consistent with the previous results as given in Refs. [13–15]. Even though the QCD theory makes the two decay constants from pseudoscalar current and axial current (timelike component) identical, i.e., $\mathcal{C}_p = \mathcal{C}_{a,0}$. Here we have examined this point by the independent calculation of the pseudoscalar decay constants. On the other hand, the results for vector B_c meson decay constant and its matching coefficient are novel. In the limit of $m_b = m_c = m_Q$, our result for the vector current agrees with the previous results in literature [22,45].

For the pseudoscalar meson B_c and vector meson B_c^*, the leptonic decay widths can be written as

$$\Gamma(B_c^+ \to l^+\nu_l) = \frac{|V_{bc}|^2}{8\pi} G_F^2 m_{B_c} m_l^2 \left(1 - \frac{m_l^2}{m_{B_c}^2}\right)^2 f_{B_c}^{p\,2}, \tag{28}$$

$$\Gamma(B_c^{*+} \to l^+\nu_l) = \frac{|V_{bc}|^2}{12\pi} G_F^2 m_{B_c^*}^3 \left(1 - \frac{m_l^2}{m_{B_c^*}^2}\right)^2 \cdot \left(1 + \frac{m_l^2}{2m_{B_c^*}^2}\right) f_{B_c^*}^{v\,2}. \tag{29}$$

Note that, we will evaluate $f_{B_c}^p$ and $f_{B_c^*}^v$ up to a fixed order, i.e., NNLO accuracy, but when we square them, we no longer truncate the perturbative series of α_s literally up to a fixed order. To evaluate the two decay constants $f_{B_c}^p$ and $f_{B_c^*}^v$, we substitute the LDMEs in Eq. (4) with

$$\langle 0|\chi_b^\dagger \boldsymbol{\sigma} \cdot \varepsilon \psi_c|B_c^*(\mathbf{P})\rangle \approx \langle 0|\chi_b^\dagger \psi_c|B_c(\mathbf{P})\rangle \approx \sqrt{2N_c}\psi_{B_c}(0), \tag{30}$$

where $\psi_{B_c}(0)$ is the Schrödinger wave function at the origin for the B_c system and is predicted in potential models [15,65–68] as

$$|\psi_{B_c}(0)|^2 \simeq [0.10, 0.13]\ \mathrm{GeV}^3. \tag{31}$$

In Tables II–VI, we present our theoretical predictions for the decay constants $f_{B_c}^p$ and $f_{B_c^*}^v$, the leptonic decay width $\Gamma(B_c^+ \to l^+\nu_l)$ and $\Gamma(B_c^{*+} \to l^+\nu_l)$, as well as the branching ratios $\mathcal{B}(B_c^+ \to l^+\nu_l)$ and $\mathcal{B}(B_c^{*+} \to l^+\nu_l)$ with $l = (e, \mu, \tau)$. In the numerical calculations, the values of the following input parameters will be used implicitly unless otherwise stated [5]:

TABLE II. The theoretical predictions of the decay constants $f_{B_c}^p$ and $f_{B_c^*}^v$ at the LO, NLO, and NNLO level. The five input parameters are $\psi_{B_c}(0) = \sqrt{0.12^{+0.1}_{-0.2}}\ \mathrm{GeV}^{\frac{3}{2}}$, $\mu_f = 1.2^{+0.3}_{-0.2}$ GeV, $\mu = 4.75^{+1.50}_{-1.75}$ GeV, $m_b = 4.75 \pm 0.50$ GeV, and $m_c = 1.5 \pm 0.5$ GeV.

	$f_{B_c}^p$ (10^{-1} GeV)	$f_{B_c^*}^v$ (10^{-1} GeV)
LO	$4.79^{+0.20}_{-0.42}(\psi_{B_c}(0))$	$4.78^{+0.20}_{-0.42}(\psi_{B_c}(0))$
NLO	$4.37^{+0.18+0+0.03+0.03-0.07}_{-0.38-0-0.08-0.03+0.13}$	$4.15^{+0.17+0+0.05+0.03-0.07}_{-0.36-0-0.11-0.03+0.13}$
NNLO	$3.78^{+0.15-0.15+0.10+0.06+0.07}_{-0.33+0.12-0.23-0.06-0.07}$	$3.52^{+0.14-0.11+0.11+0.05+0.06}_{-0.31+0.09-0.25-0.06-0.06}$

TABLE III. The same as Table II, but for $\Gamma(B_c^+/B_c^{*+} \to e^+\nu_e)$.

	$\Gamma(B_c^+ \to e^+\nu_e)(10^{-21}\ \mathrm{GeV})$	$\Gamma(B_c^{*+} \to e^+\nu_e)(10^{-13}\ \mathrm{GeV})$
LO	$3.39^{+0.28}_{-0.56}(\psi_{B_c}(0))$	$3.45^{+0.29}_{-0.57}(\psi_{B_c}(0))$
NLO	$2.82^{+0.23+0+0.04+0.04-0.10}_{-0.47-0-0.10-0.04+0.16}$	$2.61^{+0.22+0+0.06+0.04-0.09}_{-0.43-0-0.14-0.04+0.16}$
NNLO	$2.11^{+0.18-0.16+0.11+0.06+0.08}_{-0.35+0.14-0.25-0.07-0.07}$	$1.87^{+0.16-0.12+0.12+0.05+0.06}_{-0.31+0.10-0.26-0.06-0.06}$

TABLE IV. The same as Table II, but for $\Gamma(B_c^+/B_c^{*+} \to \mu^+\nu_\mu)$.

	$\Gamma(B_c^+ \to \mu^+\nu_\mu)(10^{-16}\ \mathrm{GeV})$	$\Gamma(B_c^{*+} \to \mu^+\nu_\mu)(10^{-13}\ \mathrm{GeV})$
LO	$1.45^{+0.12}_{-0.24}(\psi_{B_c}(0))$	$3.45^{+0.29}_{-0.57}(\psi_{B_c}(0))$
NLO	$1.20^{+0.10+0+0.02+0.02-0.04}_{-0.20-0-0.04-0.02+0.07}$	$2.61^{+0.22+0+0.06+0.04-0.09}_{-0.43-0-0.14-0.04+0.16}$
NNLO	$0.90^{+0.08-0.07+0.05+0.03+0.03}_{-0.15+0.06-0.11-0.03-0.03}$	$1.87^{+0.16-0.12+0.12+0.05+0.06}_{-0.31+0.10-0.26-0.06-0.06}$

TABLE V. The same as Table II, but for $\Gamma(B_c^+/B_c^{*+} \to \tau^+\nu_\tau)$.

	$\Gamma(B_c^+ \to \tau^+\nu_\tau)(10^{-14}\ \mathrm{GeV})$	$\Gamma(B_c^{*+} \to \tau^+\nu_\tau)(10^{-13}\ \mathrm{GeV})$
LO	$3.47^{+0.29}_{-0.58}(\psi_{B_c}(0))$	$3.04^{+0.25}_{-0.51}(\psi_{B_c}(0))$
NLO	$2.88^{+0.24+0+0.05+0.04-0.10}_{-0.48-0-0.10-0.04+0.17}$	$2.30^{+0.19+0+0.06+0.03-0.08}_{-0.38-0-0.12-0.03+0.14}$
NNLO	$2.16^{+0.18-0.17+0.11+0.07+0.08}_{-0.36+0.14-0.26-0.07-0.08}$	$1.65^{+0.14-0.10+0.10+0.05+0.05}_{-0.27+0.09-0.23-0.05-0.05}$

$$V_{cb} = 0.0408, \quad G_F = 1.16638 \times 10^{-5}\ \mathrm{GeV}^{-2},$$
$$m_e = 0.511\ \mathrm{MeV}, \quad m_\mu = 0.10566\ \mathrm{GeV},$$
$$m_\tau = 1.777\ \mathrm{GeV}, \quad m_{B_c} = 6.274\ \mathrm{GeV}, \quad \tau_{B_c} = 0.51\ \mathrm{ps}. \tag{32}$$

For the vector B_c^* meson, there are many theoretical predictions for its mass and decay widths [33,69,70]. We here use the following values as given in Refs. [69,71]

$$m_{B_c^*} = 6.314\ \mathrm{GeV}, \quad \Gamma_{\mathrm{tot}}(B_c^*) = 0.08 \times 10^{-6}\ \mathrm{GeV}. \tag{33}$$

From the numerical results as listed in Tables III–VI, one see the following points:

(1) For the three $B_c^+ \to l^+\nu_l$ decay modes, the electronic, muonic, and tauonic decay widths are around the order of 10^{-21} GeV, 10^{-16} GeV, and 10^{-14} GeV, respectively, due to the strong m_l^2 suppression as can be seen from Eq. (28).

TABLE VI. The same as Table II, but for the branching ratios of $B_c^+/B_c^{*+} \to l^+\nu_l$ with $l^+ = (e^+, \mu^+, \tau^+)$ at the NNLO level.

	$e^+\nu_e$	$\mu^+\nu_\mu$	$\tau^+\nu_\tau$
B_c	$(1.64^{+0.44}_{-0.71}) \times 10^{-9}$	$(7.00^{+1.89}_{-3.01}) \times 10^{-5}$	$(1.68^{+0.45}_{-0.72}) \times 10^{-2}$
B_c^*	$(2.34^{+0.61}_{-1.01}) \times 10^{-6}$	$(2.34^{+0.61}_{-1.01}) \times 10^{-6}$	$(2.06^{+0.54}_{-0.89}) \times 10^{-6}$

(2) For each kind of the leptonic decay mode, the decay width $\Gamma(B_c^+ \to l^+\nu_l)$ will become smaller moderately when higher-order corrections are taken into account,

$$\Gamma^{\mathrm{LO}}|_{B_c^+ \to l^+\nu_l} : \Gamma^{\mathrm{NLO}} : \Gamma^{\mathrm{NNLO}} \approx 1 : 0.83 : 0.62, \tag{34}$$

for $l^+ = (e^+, \mu^+, \tau^+)$, respectively.

(3) For similar B_c^* leptonic decays, the decay width $\Gamma(B_c^{*+} \to l^+\nu_l)$ with $l^+ = (e^+, \mu^+, \tau^+)$ are always around 10^{-13} GeV. Numerically, $\Gamma(B_c^{*+} \to e^+\nu_e) = \Gamma(B_c^{*+} \to \mu^+\nu_\mu)$ up to the NNLO level and

$$\frac{\Gamma(B_c^{*+} \to \tau^+\nu_\tau)}{\Gamma(B_c^{*+} \to \mu^+\nu_\mu)} \approx 0.88, \tag{35}$$

$$\Gamma^{\mathrm{LO}}|_{B_c^{*+} \to l^+\nu_l} : \Gamma^{\mathrm{NLO}} : \Gamma^{\mathrm{NNLO}} \approx 1 : 0.76 : 0.54. \tag{36}$$

(4) The leptonic branching ratios for $B_c^{*+} \to l^+\nu_l$ decays at the NNLO level are around 2.1×10^{-6} for all three kinds of leptonic decay channels. For $B_c^+ \to l^+\nu_l$ decays, however, there is a very large difference between the branching ratios for the different decay modes; from the order of 10^{-9} for $\mathcal{B}(B_c^+ \to e^+\nu_e)$ decay to 10^{-5} and 10^{-2} for the muonic and tauonic decay mode, respectively.

Considering the hadronic production of B_c and B_c^* has a large uncertainty and their cross sections at the LHC are from tens to hundreds of nanobarn [72–74], there are tens to hundreds $B_c^{*+} \to l^+ + \nu_l$ events, while hundreds to thousands $B_c^+ \to \mu^+ + \nu_\mu$ events at the LHC for 1 fb^{-1} proton-proton collision data at a center-of-mass energy of 14 TeV. Of course, the branching ratio of $B_c^+ \to \tau^+ + \nu_\tau$ is around three orders larger than the branching ratio of $B_c^+ \to \mu^+ + \nu_\mu$; thus this channel shall also be a good channel to detect B_c meson if the reconstruction of the final state tau lepton is well-controlled. In total, we expect these leptonic decay channels for both B_c and B_c^* can be accessible at the LHC precision experiments.

V. CONCLUSION

In this paper, we have performed a NNLO calculation of the decay constants of the beauty-charmed meson B_c and B_c^*. The NNLO result for vector current decay constant is novel. The updated leptonic decay branching ratios combined with the latest extraction of the NRQCD LDMEs of the B_c meson will be tested in future experiments. Through the careful studies of the decay constants of B_c meson, one can expect that more and more decay channels of beauty-charmed mesons are accessible and their absolute branching ratios can also be measured. The novel results of the anomalous dimension for the vector current in the NRQCD shall provide more information on the renormalization properties of the NRQCD LDMEs. The carefully studied NNLO matching coefficients are also helpful to investigate the behaviors of the B_c meson decays when the doubly heavy quarks are in their threshold region.

ACKNOWLEDGMENTS

We thank L. B. Chen, J. B. He, Y. M. Li, X. Liu, W. L. Sang and C. Y. Wang for many useful discussions. This work is supported by NSFC under Grants No. 11775117 and No. 12075124, and by Natural Science Foundation of Jiangsu under Grant No. BK20211267.

Note added.—After our manuscript was submitted to the journal, a new preprint [75] appeared investigating the same subject at next-to-next-to-next-to-leading order, in which the NNLO matching coefficient for the decay constant of B_c^* is consistent with our result.

APPENDIX: THE WAVE FUNCTION AND MASS RENORMALIZATION CONSTANTS

Allowing for n_b quarks with mass m_b, n_c quarks with mass m_c and n_l massless quarks appearing in the quark loop, the analytic expression of bottom quark on shell wave function renormalization constant $Z_{2,b}$ up to NNLO is of the following form

$$
\begin{aligned}
Z_{2,b} = {} & 1+\frac{\alpha_s}{\pi}C_F\left\{-\frac{3}{4\epsilon}-\frac{3}{4}\ln\frac{\mu^2}{m_b^2}-1-\frac{\epsilon}{16}\left(6\ln^2\frac{\mu^2}{m_b^2}+16\ln\frac{\mu^2}{m_b^2}+\pi^2+32\right)\right.\\
& \left.-\epsilon^2\left[\frac{1}{8}\ln^3\frac{\mu^2}{m_b^2}+\frac{1}{2}\ln^2\frac{\mu^2}{m_b^2}+\left(2+\frac{\pi^2}{16}\right)\ln\frac{\mu^2}{m_b^2}-\frac{\zeta_3}{4}+\frac{\pi^2}{12}+4\right]\right\}\\
& +\frac{\alpha_s^2}{\pi^2}C_F\left\{C_F\left[\frac{9}{32\epsilon^2}+\frac{1}{192\epsilon}\left(108\ln\frac{\mu^2}{m_b^2}+153\right)+\frac{9}{16}\ln^2\frac{\mu^2}{m_b^2}+\frac{51}{32}\ln\frac{\mu^2}{m_b^2}+\pi^2\ln 2-\frac{3\zeta_3}{2}-\frac{49\pi^2}{64}+\frac{433}{128}\right]\right.\\
& +C_A\left[\frac{11}{32\epsilon^2}-\frac{127}{192\epsilon}-\frac{11}{32}\ln^2\frac{\mu^2}{m_b^2}-\frac{215}{96}\ln\frac{\mu^2}{m_b^2}-\frac{1}{2}\pi^2\ln 2+\frac{3\zeta_3}{4}+\frac{5\pi^2}{16}-\frac{1705}{384}\right]\\
& +T_F n_b\left[\frac{1}{16\epsilon}\left(4\ln\frac{\mu^2}{m_b^2}+1\right)+\frac{3}{8}\ln^2\frac{\mu^2}{m_b^2}+\frac{11}{24}\ln\frac{\mu^2}{m_b^2}-\frac{5\pi^2}{16}+\frac{947}{288}\right]\\
& +T_F n_c\left[\frac{1}{16\epsilon}\left(4\ln\frac{\mu^2}{m_b^2}-8\ln x+1\right)+\frac{\pi^2x^4}{4}-\frac{5\pi^2x^3}{8}+\frac{7x^2}{4}-\frac{3\pi^2x}{8}+\frac{3}{8}\ln^2\frac{\mu^2}{m_b^2}+\frac{11}{24}\ln\frac{\mu^2}{m_b^2}\right.\\
& +\ln(x)\ln(x+1)\left(-\frac{3x^4}{2}-\frac{5x^3}{4}-\frac{3x}{4}-\frac{1}{2}\right)+\mathrm{Li}_2(x)\left(-\frac{3x^4}{2}+\frac{5x^3}{4}+\frac{3x}{4}-\frac{1}{2}\right)\\
& +\ln^2(x)\left(\frac{3x^4}{2}+1\right)-\mathrm{Li}_2(-x)\left(\frac{3x^4}{2}+\frac{5x^3}{4}+\frac{3x}{4}+\frac{1}{2}\right)\\
& \left.+\ln(x)\left(x^2-\ln\frac{\mu^2}{m_b^2}-\ln(1-x)\left(\frac{3x^4}{2}-\frac{5x^3}{4}-\frac{3x}{4}+\frac{1}{2}\right)+\frac{2}{3}\right)+\frac{5\pi^2}{48}+\frac{443}{288}\right]\\
& \left.+T_F n_l\left[\frac{-1}{8\epsilon^2}+\frac{11}{48\epsilon}+\frac{1}{8}\ln^2\frac{\mu^2}{m_b^2}+\frac{19}{24}\ln\frac{\mu^2}{m_b^2}+\frac{\pi^2}{12}+\frac{113}{96}\right]\right\}. \qquad \text{(A1)}
\end{aligned}
$$

Similarly, the charm quark on shell wave function renormalization constant $Z_{2,c}$ up to NNLO can be obtained by the direct replacement of some relevant parameters in $Z_{2,b}$

$$Z_{2,c} = Z_{2,b}|_{m_b \to m_c; x \to \frac{1}{x}; n_b \leftrightarrow n_c}. \tag{A2}$$

The bottom and charm quark on shell mass renormalization constant $Z_{m,b}$ and $Z_{m,c}$ up to NNLO can be written in the following form

$$\begin{aligned}
Z_{m,b} = 1 &+ \frac{\alpha_s}{\pi} C_F \Bigg\{ -\frac{3}{4\epsilon} - \frac{3}{4} \ln \frac{\mu^2}{m_b^2} - 1 - \frac{\epsilon}{16} \left(6 \ln^2 \frac{\mu^2}{m_b^2} + 16 \ln \frac{\mu^2}{m_b^2} + \pi^2 + 32 \right) \\
&- \epsilon^2 \left[\frac{1}{8} \ln^3 \frac{\mu^2}{m_b^2} + \frac{1}{2} \ln^2 \frac{\mu^2}{m_b^2} + \left(2 + \frac{\pi^2}{16} \right) \ln \frac{\mu^2}{m_b^2} - \frac{\zeta_3}{4} + \frac{\pi^2}{12} + 4 \right] \Bigg\} \\
&+ \frac{\alpha_s^2}{\pi^2} C_F \Bigg\{ C_F \left[\frac{9}{32\epsilon^2} + \frac{1}{192\epsilon} \left(108 \ln \frac{\mu^2}{m_b^2} + 135 \right) + \frac{9}{16} \ln^2 \frac{\mu^2}{m_b^2} + \frac{45}{32} \ln \frac{\mu^2}{m_b^2} + \frac{1}{2} \pi^2 \ln 2 - \frac{3\zeta_3}{4} - \frac{17\pi^2}{64} + \frac{199}{128} \right] \\
&+ C_A \left[\frac{11}{32\epsilon^2} - \frac{97}{192\epsilon} - \frac{11}{32} \ln^2 \frac{\mu^2}{m_b^2} - \frac{185}{96} \ln \frac{\mu^2}{m_b^2} - \frac{1}{4} \pi^2 \ln 2 + \frac{3\zeta_3}{8} + \frac{\pi^2}{12} - \frac{1111}{384} \right] \\
&+ T_F n_b \left[\frac{-1}{8\epsilon^2} + \frac{5}{48\epsilon} + \frac{1}{8} \ln^2 \frac{\mu^2}{m_b^2} + \frac{13}{24} \ln \frac{\mu^2}{m_b^2} - \frac{\pi^2}{6} + \frac{143}{96} \right] \\
&+ T_F n_c \Bigg[\frac{-1}{8\epsilon^2} + \frac{5}{48\epsilon} + \frac{x^4}{2} \ln^2 x + \frac{\pi^2 x^4}{12} - \frac{\pi^2 x^3}{4} + \frac{3x^2}{4} - \frac{\pi^2 x}{4} + \frac{1}{8} \ln^2 \frac{\mu^2}{m_b^2} + \frac{13}{24} \ln \frac{\mu^2}{m_b^2} \\
&+ \ln(x) \ln(x+1) \left(-\frac{x^4}{2} - \frac{x^3}{2} - \frac{x}{2} - \frac{1}{2} \right) + \mathrm{Li}_2(x) \left(-\frac{x^4}{2} + \frac{x^3}{2} + \frac{x}{2} - \frac{1}{2} \right) \\
&- \mathrm{Li}_2(-x) \left(\frac{x^4}{2} + \frac{x^3}{2} + \frac{x}{2} + \frac{1}{2} \right) + \ln(x) \left(\frac{x^2}{2} - \ln(1-x) \left(\frac{x^4}{2} - \frac{x^3}{2} - \frac{x}{2} + \frac{1}{2} \right) \right) + \frac{\pi^2}{12} + \frac{71}{96} \Bigg] \\
&+ T_F n_l \left[\frac{-1}{8\epsilon^2} + \frac{5}{48\epsilon} + \frac{1}{8} \ln^2 \frac{\mu^2}{m_b^2} + \frac{13}{24} \ln \frac{\mu^2}{m_b^2} + \frac{\pi^2}{12} + \frac{71}{96} \right] \Bigg\}.
\end{aligned} \tag{A3}$$

$$Z_{m,c} = Z_{m,b}|_{m_b \to m_c; x \to \frac{1}{x}; n_b \leftrightarrow n_c}. \tag{A4}$$

[1] F. Abe *et al.* (CDF Collaboration), Phys. Rev. Lett. **81**, 2432 (1998).
[2] G. Aad *et al.* (ATLAS Collaboration), Phys. Rev. Lett. **113**, 212004 (2014).
[3] A. M. Sirunyan *et al.* (CMS Collaboration), Phys. Rev. Lett. **122**, 132001 (2019).
[4] R. Aaij *et al.* (LHCb Collaboration), Phys. Rev. Lett. **122**, 232001 (2019).
[5] R. L. Workman *et al.* (Particle Data Group), Prog. Theor. Exp. Phys. **2022**, 083C01 (2022).
[6] D. Becirevic *et al.* (ETM Collaboration), Proc. Sci. LATTICE2018 (**2019**) 273.
[7] B. Colquhoun, C. T. H. Davies, J. Kettle, J. Koponen, A. T. Lytle, R. J. Dowdall, and G. P. Lepage (HPQCD Collaboration), Phys. Rev. D **91**, 114509 (2015).
[8] J. Harrison, C. T. H. Davies, and A. Lytle (HPQCD Collaboration), Phys. Rev. D **102**, 094518 (2020).
[9] G. T. Bodwin, E. Braaten, and G. P. Lepage, Phys. Rev. D **51**, 1125 (1995); **55**, 5853(E) (1997).
[10] E. Braaten and S. Fleming, Phys. Rev. D **52**, 181 (1995).
[11] C. H. Chang and Y. Q. Chen, Phys. Rev. D **49**, 3399 (1994).
[12] J. Lee, W. Sang, and S. Kim, J. High Energy Phys. 01 (2011) 113.
[13] A. I. Onishchenko and O. L. Veretin, Eur. Phys. J. C **50**, 801 (2007).
[14] L. B. Chen and C. F. Qiao, Phys. Lett. B **748**, 443 (2015).
[15] F. Feng, Y. Jia, Z. Mo, J. Pan, W. L. Sang, and J. Y. Zhang, arXiv:2208.04302.
[16] P. Marquard, J. H. Piclum, D. Seidel, and M. Steinhauser, Nucl. Phys. **B758**, 144 (2006).

[17] M. Egner, M. Fael, J. Piclum, K. Schoenwald, and M. Steinhauser, Phys. Rev. D **104**, 054033 (2021).
[18] M. Beneke, A. Signer, and V. A. Smirnov, Phys. Rev. Lett. **80**, 2535 (1998).
[19] P. Marquard, J. H. Piclum, D. Seidel, and M. Steinhauser, Phys. Lett. B **678**, 269 (2009).
[20] P. Marquard, J. H. Piclum, D. Seidel, and M. Steinhauser, Phys. Rev. D **89**, 034027 (2014).
[21] B. A. Kniehl, A. A. Penin, M. Steinhauser, and V. A. Smirnov, Phys. Rev. Lett. **90**, 212001 (2003); **91**, 139903(E) (2003).
[22] M. Egner, M. Fael, F. Lange, K. Schönwald, and M. Steinhauser, Phys. Rev. D **105**, 114007 (2022).
[23] W. L. Sang, F. Feng, Y. Jia, Z. Mo, and J. Y. Zhang, arXiv:2202.11615.
[24] F. Feng, Y. Jia, Z. Mo, J. Pan, W. L. Sang, and J. Y. Zhang, arXiv:2207.14259.
[25] X. Chen, X. Guan, C. Q. He, X. Liu, and Y. Q. Ma, arXiv:2209.14259.
[26] L. B. Chen, J. Jiang, and C. F. Qiao, J. High Energy Phys. 04 (2018) 080.
[27] W. Tao, Z. J. Xiao, and R. Zhu, Phys. Rev. D **105**, 114026 (2022).
[28] R. Y. Tang, Z. R. Huang, C. D. Lü, and R. Zhu, J. Phys. G **49**, 115003 (2022).
[29] R. Zhu, Nucl. Phys. **B931**, 359 (2018).
[30] R. Zhu, Y. Ma, X. L. Han, and Z. J. Xiao, Phys. Rev. D **95**, 094012 (2017).
[31] J. Zhao and P. Zhuang, arXiv:2209.13475.
[32] M. Bordone, A. Khodjamirian, and T. Mannel, arXiv:2209.08851.
[33] C. Sun, R. H. Ni, and M. Chen, arXiv:2209.06724.
[34] Z. J. Xiao and X. Liu, Chin. Sci. Bull. **59**, 3748 (2014).
[35] Z. G. Wang, Eur. Phys. J. A **49**, 131 (2013).
[36] J. H. Piclum, Heavy quark threshold dynamics in higher order, 10.3204/DESY-THESIS-2007-014.
[37] V. Shtabovenko, R. Mertig, and F. Orellana, Comput. Phys. Commun. **256**, 107478 (2020).
[38] F. Feng, Comput. Phys. Commun. **183**, 2158 (2012).
[39] J. Klappert, F. Lange, P. Maierhöfer, and J. Usovitsch, Comput. Phys. Commun. **266**, 108024 (2021).
[40] A. V. Smirnov and F. S. Chuharev, Comput. Phys. Commun. **247**, 106877 (2020).
[41] T. Peraro, J. High Energy Phys. 07 (2019) 031.
[42] K. G. Chetyrkin and F. V. Tkachov, Nucl. Phys. **B192**, 159 (1981).
[43] X. Liu and Y. Q. Ma, Comput. Phys. Commun. **283**, 108565 (2023).
[44] X. Liu, Y. Q. Ma, and C. Y. Wang, Phys. Lett. B **779**, 353 (2018).
[45] B. A. Kniehl, A. Onishchenko, J. H. Piclum, and M. Steinhauser, Phys. Lett. B **638**, 209 (2006).
[46] R. Bonciani and A. Ferroglia, J. High Energy Phys. 11 (2008) 065.
[47] A. I. Davydychev, P. Osland, and O. V. Tarasov, Phys. Rev. D **58**, 036007 (1998).
[48] T. de Oliveira, D. Harnett, A. Palameta, and T. G. Steele, arXiv:2208.12363.
[49] S. Bekavac, A. Grozin, D. Seidel, and M. Steinhauser, J. High Energy Phys. 10 (2007) 006.
[50] M. Fael, K. Schönwald, and M. Steinhauser, J. High Energy Phys. 10 (2020) 087.
[51] K. G. Chetyrkin, J. H. Kuhn, and C. Sturm, Nucl. Phys. **B744**, 121 (2006).
[52] W. Bernreuther and W. Wetzel, Nucl. Phys. **B197**, 228 (1982); **B513**, 758(E) (1998).
[53] P. Bärnreuther, M. Czakon, and P. Fiedler, J. High Energy Phys. 02 (2014) 078.
[54] A. G. Grozin, P. Marquard, J. H. Piclum, and M. Steinhauser, Nucl. Phys. **B789**, 277 (2008).
[55] M. A. Özcelik, Ph.D. thesis, Université Paris-Saclay, 2021.
[56] K. G. Chetyrkin, B. A. Kniehl, and M. Steinhauser, Phys. Rev. Lett. **79**, 2184 (1997).
[57] K. G. Chetyrkin, J. H. Kuhn, and M. Steinhauser, Comput. Phys. Commun. **133**, 43 (2000).
[58] A. Deur, S. J. Brodsky, and G. F. de Teramond, Nucl. Phys. **90**, 1 (2016).
[59] F. Herren and M. Steinhauser, Comput. Phys. Commun. **224**, 333 (2018).
[60] S. Abreu, M. Becchetti, C. Duhr, and M. A. Ozcelik, arXiv:2211.08838.
[61] S. Groote, J. G. Korner, and O. I. Yakovlev, Phys. Rev. D **54**, 3447 (1996).
[62] C. F. Qiao, P. Sun, D. Yang, and R. L. Zhu, Phys. Rev. D **89**, 034008 (2014).
[63] C. F. Qiao and R. L. Zhu, Phys. Rev. D **87**, 014009 (2013).
[64] C. F. Qiao, L. P. Sun, and R. L. Zhu, J. High Energy Phys. 08 (2011) 131.
[65] E. J. Eichten and C. Quigg, Phys. Rev. D **52**, 1726 (1995).
[66] V. V. Kiselev, A. E. Kovalsky, and A. I. Onishchenko, Phys. Rev. D **64**, 054009 (2001).
[67] S. M. Ikhdair and R. Sever, Int. J. Mod. Phys. A **19**, 1771 (2004).
[68] D. Shen, H. Ren, F. Wu, and R. Zhu, Int. J. Mod. Phys. A **36**, 2150135 (2021).
[69] S. Godfrey, Phys. Rev. D **70**, 054017 (2004).
[70] G. L. Wang, T. Wang, Q. Li, and C. H. Chang, J. High Energy Phys. 05 (2022) 006.
[71] B. B. Zhou, J. J. Sun, and Y. J. Zhang, Commun. Theor. Phys. **67**, 655 (2017).
[72] C. H. Chang, C. Driouichi, P. Eerola, and X. G. Wu, Comput. Phys. Commun. **159**, 192 (2004).
[73] C. H. Chang and X. G. Wu, Eur. Phys. J. C **38**, 267 (2004).
[74] C. H. Chang, J. X. Wang, and X. G. Wu, Comput. Phys. Commun. **174**, 241 (2006).
[75] W. L. Sang, H. F. Zhang, and M. Z. Zhou, arXiv:2210.02979.